

A dual-targeted multifunctional nanoformulation for potential prevention and therapy of Alzheimer's disease

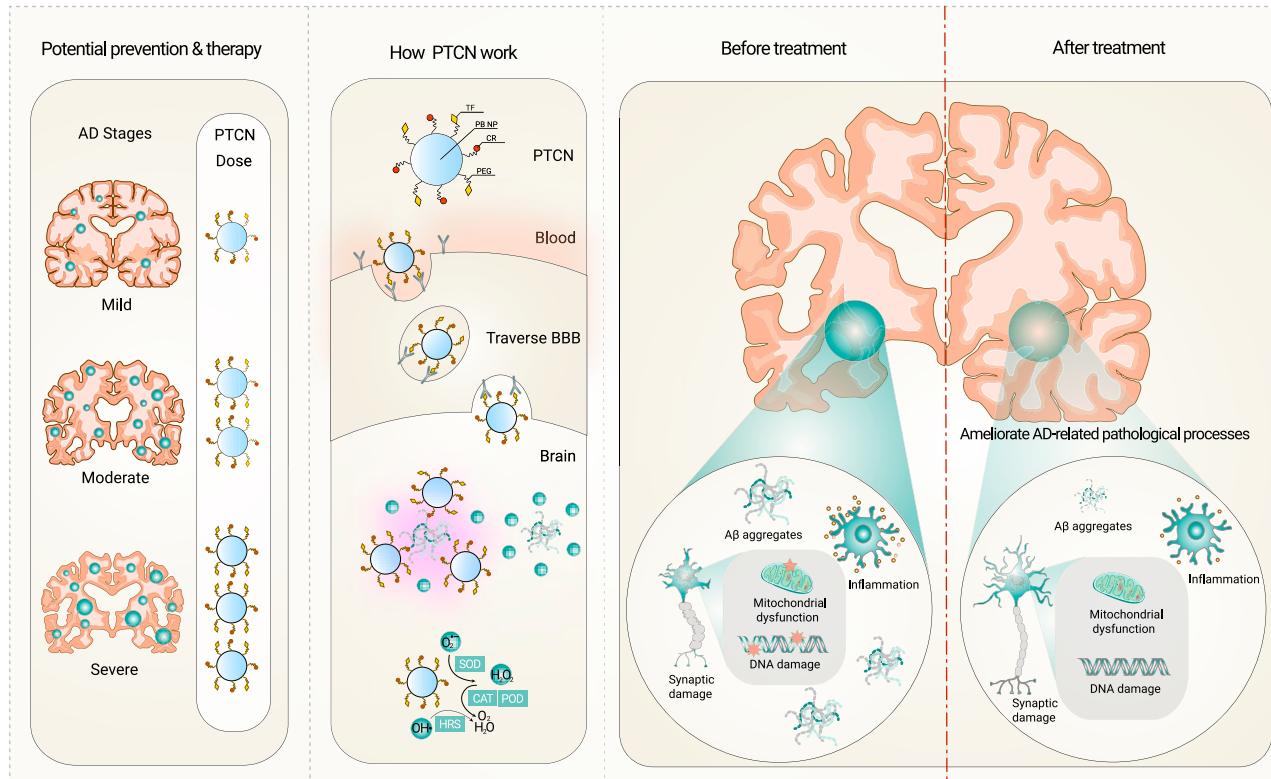
Dongju Zhao,¹ Yuqing Tang,¹ Xinjun Suo,² Chaonan Zhang,¹ Yan Dou,^{2,*} and Jin Chang^{1,*}

*Correspondence: douyan@tmu.edu.cn (Y.D.); jinchang@tju.edu.cn (J.C.)

Received: April 7, 2021; Accepted: August 27, 2021; Published Online: August 31, 2021; <https://doi.org/10.1016/j.xinn.2021.100160>

© 2021 The Authors. This is an open access article under the CC BY-NC-ND license (<http://creativecommons.org/licenses/by-nc-nd/4.0/>).

Graphical abstract



Public summary

- Dual-targeted PTCN that were assembled from traditional biomaterials can traverse the blood-brain barrier, target A_β aggregates, exert antioxidant effects and ameliorate other pathological processes
- The adjustable PTCN dosing strategy designed according to the OS level of AD stages can improve cognitive decline and hippocampal atrophy of APP/PS1 mice in both preventive and therapeutic trials
- PTCN has broad prospects for the early prevention, mild remission and late treatment of AD



Report

A dual-targeted multifunctional nanoformulation for potential prevention and therapy of Alzheimer's disease

Dongju Zhao,¹ Yuqing Tang,¹ Xinjun Suo,² Chaonan Zhang,¹ Yan Dou,^{2,*} and Jin Chang^{1,*}

¹School of Life Sciences, Tianjin University, Tianjin 300072, China

²Department of Radiology and Tianjin Key Laboratory of Functional Imaging, Tianjin Medical University General Hospital, Tianjin 300052, China

*Correspondence: douyan@tmu.edu.cn (Y.D.); jinchang@tju.edu.cn (J.C.)

Received: April 7, 2021; Accepted: August 27, 2021; Published Online: August 31, 2021; <https://doi.org/10.1016/j.xinn.2021.100160>

© 2021 The Authors. This is an open access article under the CC BY-NC-ND license (<http://creativecommons.org/licenses/by-nc-nd/4.0/>).

Citation: Zhao D., Tang Y., Suo X., et al., (2021). A dual-targeted multifunctional nanoformulation for potential prevention and therapy of Alzheimer's disease. *The Innovation* 2(4), 100160.

Antioxidation and adjustable treatment strategies are critical for the effective treatment of Alzheimer's disease (AD). Here, we design a dual-targeted Prussian blue nanoformulation (PTCN) that can cross the blood-brain barrier and target amyloid beta aggregates further exert antioxidant effects. An adjustable gradient dosing strategy with PTCN is used for the first time to design the preventive and therapeutic trials based on the severity of oxidative stress at different AD stages. The results show that PTCN could effectively ameliorate AD-related pathological processes, improve the cognitive decline, and rescue hippocampal atrophy of APP/PS1 mice in both preventive and therapeutic trials. Altogether, PTCN provided here is a successful combination of three traditional biomaterials with good biosafety, which has broad prospects for the early prevention, mild remission, and late treatment of AD, and is expected to be developed into personalized therapeutic drugs and healthcare products for clinical AD in the future.

Keywords: Alzheimer's disease; dual-targeted nanoformulation; adjustable dosing strategy; antioxidation; prevention and therapy

INTRODUCTION

Alzheimer's disease (AD) is a common neurodegenerative disease characterized by cognitive decline. However, most clinical drugs end in failure in AD treatment. Oxidative stress (OS), which refers mainly to oxidative damage induced by excessive accumulation of reactive oxygen species (ROS), plays a significant role in AD.^{1,2} The brain is highly susceptible to oxidative attacks,^{3,4} and the body's own antioxidant system normally defends against oxidative attacks to ensure low ROS levels. Under pathological conditions, endogenous antioxidants are extremely vulnerable to damage and interference, which weakens antioxidant functions in the brain. The produced ROS accumulate continuously and cannot be effectively eliminated before resulting in irreversible OS, which interacts with other pathogenic mechanisms during AD and eventually leads to cognitive impairments.^{5–7} Therefore, development of exogenous antioxidants that can combat OS is very important for AD treatment.

Many developed exogenous molecular antioxidants exhibit poor performance in cognitive function improvement for several potential reasons.^{8,9} Firstly, the blood-brain barrier (BBB) blocks access to the brain.^{10,11} Secondly, some antioxidants that entered the brain diffuse and cannot effectively concentrate in the pathological areas of AD, resulting in insufficient working concentration.¹² Nanoantioxidants can target lesions through surface modification and have been developed to treat diseases associated with OS, including AD.^{13,14} Notably, Prussian blue (PB)-associated nanoparticles (NPs) have been reported to be effective in removing ROS,^{15,16} which have been generally considered to be biosafe because the major component, PB, has been approved by the U.S. Food and Drug Administration (FDA).¹⁷ In addition, due to the simple preparation process and good reproducibility,

PB NPs have considerable potential as exogenous antioxidants for use in AD treatment.

Designing a flexible and adjustable treatment program based on the occurrence and development of AD remains a major challenge. Clinical AD is usually divided into three stages (early stage, mild; middle stage, moderate; and late stage, severe).¹⁸ Currently, most research focuses on the middle and late stages of AD, lacking intervention strategies for the early stage or even the whole disease process. OS has been proposed to be one of the causes of AD and worsens with disease progression,^{19–21} while other pathological molecules have also been found to exhibit different changes in different stages.^{22–24} Therefore, flexible and adjustable antioxidant treatment based on the different degrees of OS in different AD stages would help alleviate other pathologies and enable personalized treatment of AD.

Herein, a dual-targeted PB@PEG-TF/CR NPs (PTCN) was assembled from traditional biomaterials and administrated using an antioxidation-guided adjustable dosing strategy for potential prevention and therapy of AD. The PB NPs in PTCN can exert antioxidant effects to scavenge ROS, and surface modification with transferrin (TF) and Congo red (CR) enables to traverse the BBB and target amyloid beta (A β) aggregates, respectively.^{25–27} The designed antioxidation-guided adjustable dosing strategy with PTCN can effectively attenuate OS in the hippocampus, thereby ameliorating other pathological processes and ultimately improving the cognitive functions and rescuing hippocampal atrophy for both preventive and therapeutic trials of APP/PS1 mice. Altogether, this work reveals the potential of PTCN to be developed as a promising drug and healthcare product for clinical personalized treatment of AD, realizing the early prevention, mild remission, and late treatment of AD.

RESULTS AND DISCUSSION

Synthesis and characterization of PTCN

PTCN was synthesized by simultaneous surface modification of carboxylated PEGylated PB NPs (PB@PEG NPs) with TF and CR (Figure S1). Transmission electron microscopy (TEM) images showed that PTCN exhibited a clear spherical shape and good uniformity (Figure 1A). The hydrodynamic diameter and zeta potential of PTCN (198 ± 18.27 nm, -15.97 ± 0.28 mV) (Figure S2) were larger than those of PB@PEG NPs (88.79 ± 4.50 nm, -35.83 ± 0.23 mV) (Figure S3). Moreover, PTCN exhibited a TF characteristic peak at 270 nm and CR characteristic peaks at both 350 and 500 nm in UV-vis-NIR spectra (Figure 1B). These results indicated that PB@PEG NPs were successfully modified with TF and CR. Notably, the hydrodynamic diameter of PTCN showed no significant changes for 14 days, indicating its excellent stability for further application (Figure S4).

Next, we verified two important functions of PTCN, including crossing of the BBB and targeting of A β aggregates in the brain. TF modification has been widely demonstrated to help NPs cross the BBB via TF receptor-mediated endocytosis.²⁸ To demonstrate TF-mediated BBB crossing function of PTCN, a compact monolayer of mouse brain endothelial cells (bEnd.3)

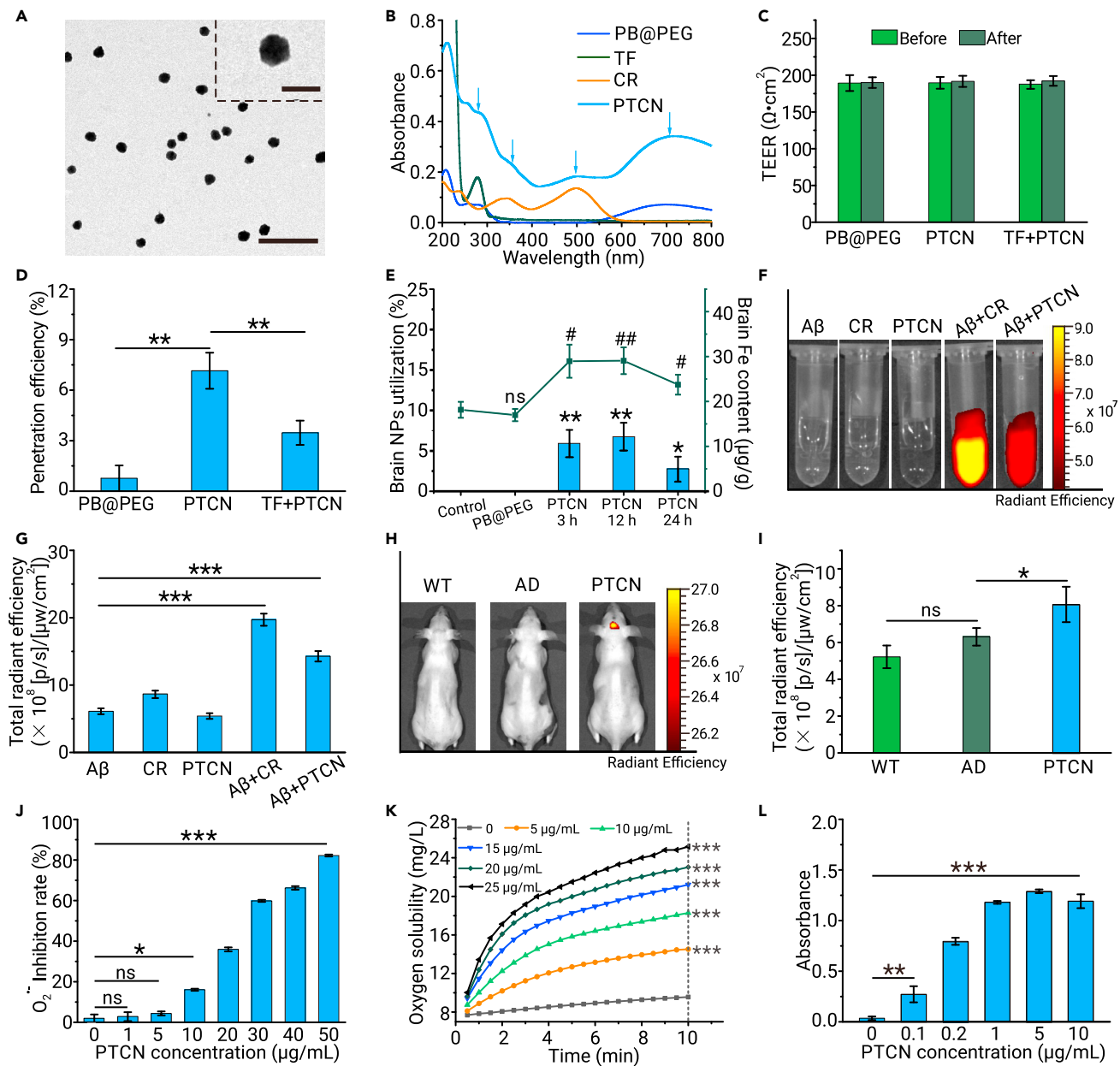


Figure 1. Characterization and ROS-scavenging ability of PTCN (A) TEM images of PTCN. Scale bars, 1 μm , 200 nm (inset). (B) UV-vis-NIR absorption spectra. (C) Transendothelial electrical resistance (TEER) values of the bEnd.3 cell monolayer before and after sample incubation. (D) Penetration efficiency (%) of PTCN crossing the *in vitro* BBB transwell model. (E) Brain NPs utilization (%) and average brain Fe content ($\mu\text{g}/\text{g}$) analysis. *Compared with the PB@PEG group; #compared with control group. Three mice per group ($n = 3$). (F) Fluorescence images and (G) fluorescence intensity of A β aggregates ($100 \mu\text{M}$) binding to PTCN ($20 \mu\text{g}/\text{mL}$) as determined by an *in vivo* imaging system. (H and I) (H) *In vivo* fluorescence images and (I) fluorescence intensity after intravenous administration of PTCN to APP/PS1 mice. (J) The SOD mimetic activity was measured via the scavenging $\text{O}_2^{\cdot-}$ in the presence of PTCN. (K) CAT-like activity was investigated via the increased oxygen solubility after incubating PTCN with H_2O_2 . *Compared with non-PTCN incubated group (gray line). (L) POD-like activity was investigated by detecting the absorption of H_2O_2 -mediated TMB oxidation products at 650 nm. For all graphs, the data are presented as the mean \pm SD and statistical significance was calculated by two-tailed t test; * $p < 0.05$, ** $p < 0.01$, *** $p < 0.001$, # $p < 0.05$, #* $p < 0.01$.

was implanted into transwell filters. Transendothelial electrical resistance values during the experiments were all above $180 \Omega \cdot \text{cm}^2$, indicating the membrane integrity (Figure 1C). After 12 h incubation of NPs, 7.2% of PTCN penetrated through the bEnd.3 monolayers, which was obviously higher than 0.8% of PB@PEG NPs (Figure 1D). After excess free TF was pre-incubated to block TF receptor-mediated endocytosis, the penetration efficiency of PTCN was reduced to 3.5%, indicating that TF receptor-mediated endocytosis played a key role in the penetration process of PTCN. Then, on the basis of removing the endogenous Fe content in the untreated control group, the efficiency of PTCN entering the brain was evaluated by quantitative analysis of the increased Fe content in the brain. The results showed that the

brain utilization of PTCN was approximately 5.9% at 3 h post-injection, reached the peak at 12 h post-injection, and retained 24 h after injection, while that of NPs without TF modification was almost zero (Figure 1E). In addition to brain utilization, the mass fraction of Fe in the brain was calculated; the results showed that PTCN increased the brain average Fe content by 90% 3 h after injection, which was significantly higher than the control group (Figure 1E). Furthermore, the presence of PTCN in hippocampal tissues of APP/PS1 mice at 3 h post-injection was further confirmed by biological TEM. Unmodified PB@PEG NPs were found in blood vessels but not in the hippocampus, demonstrating that PB@PEG NPs without TF modification cannot pass through the BBB into the brain (Figure S5). As expected,

PTCN was observed not only in blood vessels but also in the hippocampus. In particular, we not only observed the presence of PTCN on the luminal side of endothelial cells but also the efflux of PTCN on the abluminal side of the BBB, intuitively showing that PTCN can penetrate to the hippocampus from the blood vessels. These results strongly demonstrate that TF-modified PTCN can effectively cross the BBB, enter the brain, and enrich in the hippocampus of mice.

What's more, it has been reported that CR can be specifically bound to A β aggregates by unique hydrogen bonds and that the resulting CR-A β complex greatly enhances the red fluorescence of CR,²⁷ which is typically weak. To verify this specific binding of PTCN with A β aggregates, the fluorescence intensities of PTCN and CR combined with A β aggregates were measured and compared with those of free CR and A β aggregates alone. After binding with A β aggregates, both PTCN and CR showed significantly heightened fluorescence intensities, and the fluorescence intensity of PTCN combined with 100 μ M A β aggregates was approximately 1.5 times stronger than that of PTCN alone (Figure S6). Under an inverted fluorescence microscope, only these complexes were clearly observed and had greatly enhanced red fluorescence (Figure S7). Furthermore, the *in vitro* fluorescence of the PTCN-A β complex was also evaluated by an *in vivo* imaging system. The fluorescence enhancement of the PTCN-A β complex was not significantly less than that of the CR-A β complex (Figures 1F and 1G). Then *in vivo* fluorescence imaging was performed on APP/PS1 mice with high levels of A β aggregates in the brain, and demonstrated that only PTCN-treated APP/PS1 mice showed strong fluorescence signals in the brain region, but not in other organs (Figures 1H and 1I), indicating that fluorescence was only visible when the CR on PTCN bound to A β in the brain. All these results confirm that PTCN can pass through the BBB and specifically combine with A β aggregates.

ROS-scavenging ability of PTCN

The ROS-scavenging ability of PTCN is essential for its effective antioxidant activity in the treatment of AD. Therefore, we investigated the ability of PTCN to act like multiple enzymes, including superoxide dismutase (SOD), catalase (CAT), and peroxidase (POD), as well as its hydroxyl radical scavenging (HRS) activity.^{25,28} These types of activity are key to removal of ROS. First, SOD-like activity was evaluated via assessment of O₂⁻ scavenging. Excessive O₂⁻ was generated by the xanthine/xanthine oxidase system and detected by formazan formation using a WST-8 assay kit. The O₂⁻ inhibition rate gradually increased with PTCN concentration (Figure 1J), indicating good SOD-like activity of PTCN. Second, since O₂⁻ can be dismuted spontaneously or catalyzed by SOD to form H₂O₂, which is another important ROS, H₂O₂ scavenging was used to evaluate CAT-like activity and POD-like activity. CAT-like activity was investigated via assessment of H₂O₂ decomposition to produce O₂. After PTCN was added into 30% H₂O₂ solution, the amount of bubbles increased with PTCN concentration, while PTCN alone did not exhibit bubbles (Figure S8). Quantitative analysis of dissolved oxygen showed that PTCN catalyzed production of O₂ from H₂O₂ in a concentration- and time-dependent manner (Figure 1K). Furthermore, POD-like activity was investigated by catalyzing the reaction of H₂O₂ with the natural substrate 3,5,3',5'-tetramethylbenzidine (TMB). PTCN treatment resulted in the characteristic absorbance of the products of H₂O₂-mediated TMB oxidation at 650 nm, and the effect increased with the PTCN concentration (Figure 1L). These results confirmed the good CAT-like activity and POD-like activity of PTCN. Finally, HRS activity was evaluated via assessment of scavenging of ·OH, which is considered to be an initiator of lipid peroxidation. A TiO₂/UV system was chosen to generate ·OH, which was trapped by 5,5-dimethyl-pyrroline-N-oxide (DMPO) and detected by electron spin resonance. The signal intensity of DMPO-·OH was progressively reduced with increasing PTCN concentrations, suggesting a direct scavenging effect of PTCN on ·OH (Figure S9). These results reveal that all the enzyme-like activities of PTCN exhibit concentration dependence and that PTCN is an effective antioxidant with ROS-scavenging activity.

It is generally believed that iron-based NPs can react with H₂O₂ to cause Fenton reaction and produce ·OH, thus mediating biotoxicity.²⁹ Therefore,

the assessment of whether PTCN can undergo Fenton reaction was crucial for the correct evaluation of ROS-scavenging activity and the potential biosafety of PTCN. As shown in Figure S10, the FeSO₄ and H₂O₂ system has been considered a classic Fenton reaction model, and the produced ·OH could specifically react with salicylic acid to form 2,3-dihydroxybenzoic acid, exhibiting an obvious UV absorption peak at 510 nm.³⁰ However, there was no absorption peak at 510 nm representing ·OH generation observed after replacing FeSO₄ with PTCN. Our results demonstrated that PTCN had no Fenton-like activity, which was similar to previous studies.^{25,31} Furthermore, considering that the chemical stability of PTCN in acidic solutions was not negligible for the efficiency of antioxidant activity and TF-mediated BBB crossing, we further assessed the possible iron release from PTCN as well as the detachment of targeting groups in the lysosomal mimic fluid. Acetate buffer, pH 3.6, was used to mimic lysosomal-like acidic condition, and PTCN was incubated with this buffer for 48 h, and then the suspension was centrifuged to obtain precipitate and supernatant. After replacing FeSO₄ in the Fenton reaction model with the supernatant and precipitate of PTCN, no absorption peak at 510 nm was observed, and the characteristic absorption peak of PB at 700 nm was still observed in the precipitation (Figure S10), demonstrating that the structure of PB as the core component of PTCN was not affected and that no iron was released from the PTCN in the lysosomal mimic fluid. In addition, the characteristic peaks of TF, CR, and PB were still retained in the precipitate, but not found in the supernatant (Figure S11), indicating that targeting groups were not detached from PTCN in the lysosomal mimic fluid.

Antioxidant and neuroprotective effects of PTCN in PC12 cells

To test whether ROS scavenging by PTCN could provide neuroprotection, we evaluated the effect of PTCN on the viability of PC12 cells under H₂O₂ oxidative shock.³² Cytotoxicity tests were first carried out on PTCN. Among the components of PTCN, PB and TF have been approved by the FDA, and CR shows very low cytotoxicity (Figure S12). Cell viability after treatment with PTCN, at all studied concentrations, exceeded 80%, indicating PTCN's low cytotoxicity (Figure S13). Then, H₂O₂ was used for oxidative shock to construct a cell model of OS. Oxidative shock significantly reduced cell viability, with greater effects at higher H₂O₂ concentrations (Figure 2A). To assess the therapeutic effects of PTCN on cells under oxidative shock, cells were first treated with H₂O₂ and then with PTCN. Cell viability was obviously lower in H₂O₂-treated cells than in untreated control cells, and the reduction was exacerbated with increasing H₂O₂ concentrations (Figure 2B). PTCN posttreatment greatly rescued the cell viability, resulting in even higher viability in the posttreatment group than in the control group (Figure 2B), which may have been attributable to the oxygen produced through H₂O₂ decomposition. To assess the preventive effects of PTCN on oxidative shock in cells, cells were treated with PTCN and then with H₂O₂. PTCN pretreatment also greatly enhanced cell viability, as the viability was greater in pretreated cells subjected to oxidative shock than in the cells subjected to oxidative shock alone, and the effect increased with increasing PTCN concentration (Figure 2C). These results indicate that PTCN posttreatment and pretreatment can effectively rescue cells and prevent the cell death caused by H₂O₂ oxidative shock, respectively.

Then, the effects of PTCN posttreatment and pretreatment on cellular ROS levels and apoptosis under H₂O₂ oxidative shock were further studied. DCFH-DA staining was performed to measure cellular ROS levels. Unlike the control treatment and PTCN alone, H₂O₂ treatment caused excess ROS production in cells and resulted in shrunken cells and decreased numbers of synapses (Figures 2D and 2E). PTCN posttreatment and pretreatment restored the morphology of cells and synapses, while reducing the elevations in ROS levels caused by H₂O₂ oxidative shock (Figures 2D and S14). These results were further demonstrated by flow cytometric quantitative fluorescence analysis (Figures 2E and S15). Dual staining with Calcein-AM and propidium iodide was performed to mark live and dead cells. The results showed that cells were destroyed after H₂O₂ oxidative shock, while PTCN posttreatment and pretreatment prevented the cells from being damaged (Figure S16). Moreover, flow cytometric quantitative apoptosis analysis demonstrated that

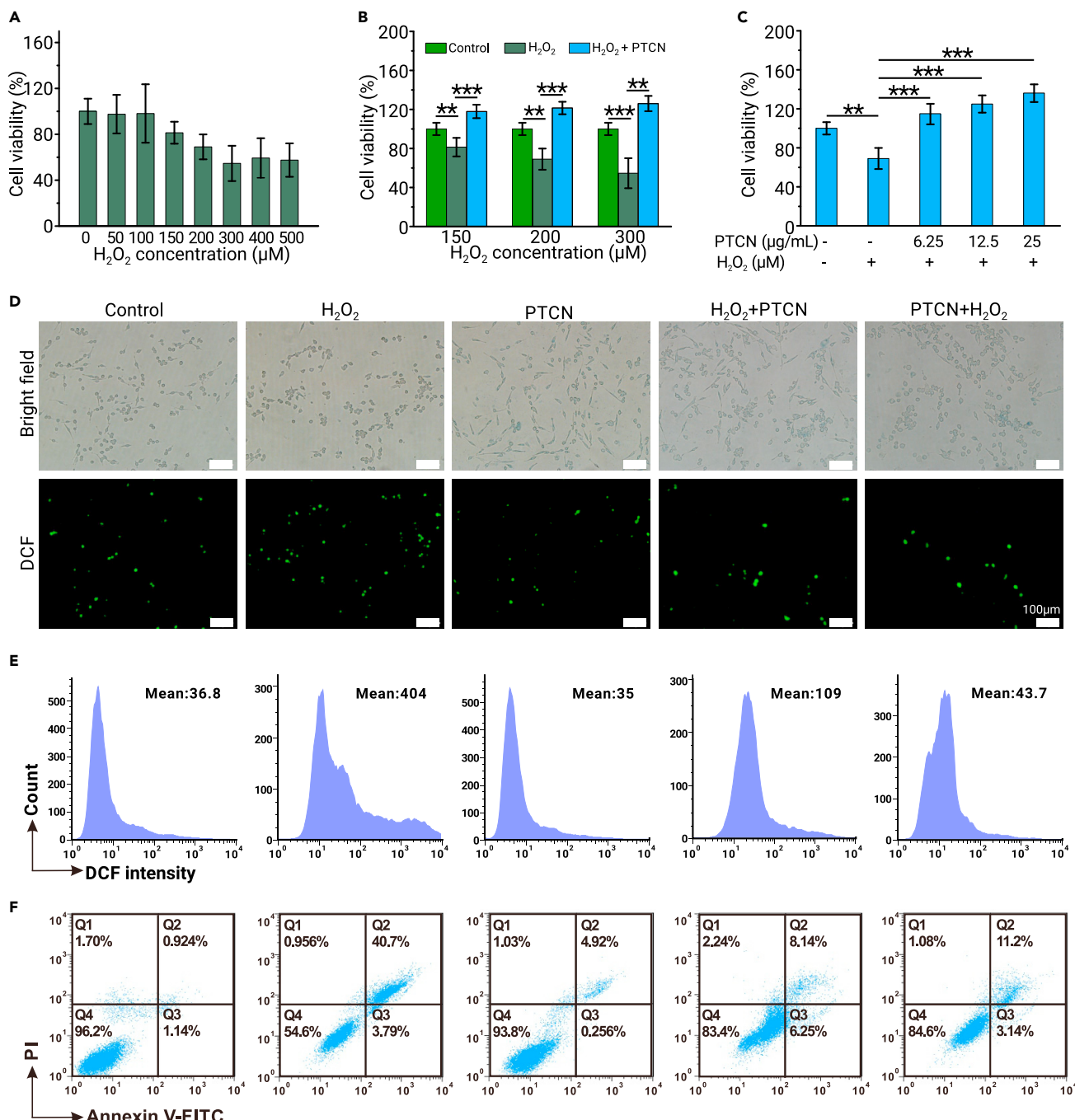


Figure 2. Antioxidant and neuroprotective effects of PTCN in PC12 cells (A) Viability of PC12 cells after incubation with H₂O₂ at different concentrations. (B) Rescue effect of PTCN on the viability of PC12 cells treated with different concentrations of H₂O₂ and then incubated with PTCN (12.5 μg/mL). (C) Rescue effect of PTCN on the viability of PC12 cells treated with different concentrations of PTCN and then incubated with H₂O₂ (200 μM). (D) DCFH-DA staining images of PC12 cells after different treatments (green, ROS). Scale bars, 100 μm. (E) Flow cytometry analysis of ROS levels in PC12 cells as determined by DCFH-DA staining. (F) Flow cytometry analysis of apoptosis. For all graphs, the data are presented as the mean ± SD and statistical significance was calculated by two-tailed t test; *p < 0.05, **p < 0.01, ***p < 0.001.

PTCN posttreatment significantly improved the survival rate from 54.6% (under H₂O₂ oxidative shock) to 83.4%; similarly, PTCN pretreatment increased the survival rate to 84.6% (Figure 2F). These results suggest that PTCN provides excellent neuroprotection against oxidative shock for both preventive and therapeutic treatments.

Behavioral and hippocampal volume assessment for evaluation of the efficacy of PTCN for AD prevention and therapy *in vivo*

Before *in vivo* treatments, the biosafety of PTCN was demonstrated by hematoxylin and eosin staining (Figure S17) and routine blood analysis (Table

S1). Next, we quantitatively analyzed Fe content in the blood of APP/PS1 mice after intravenous injection of PTCN using ICP-MS. As shown in Figure S18, we observed high blood Fe content at 0.5 h post-injection and a decrease of only 33% at 48 h post-injection, suggesting that PTCN composed mainly of Fe might have longer blood circulation. On the basis of the brain utilization and blood Fe content of PTCN, we designed a gradient dosing strategy for the preventive and therapeutic trials with APP/PS1 mice according to the severity of OS in different AD stages (Figures 3A and S19). For the preventive trial, APP/PS1 mice at the age of 10 weeks were treated with a low dose of PTCN until 16 weeks and then with a medium dose until 22 weeks, while,

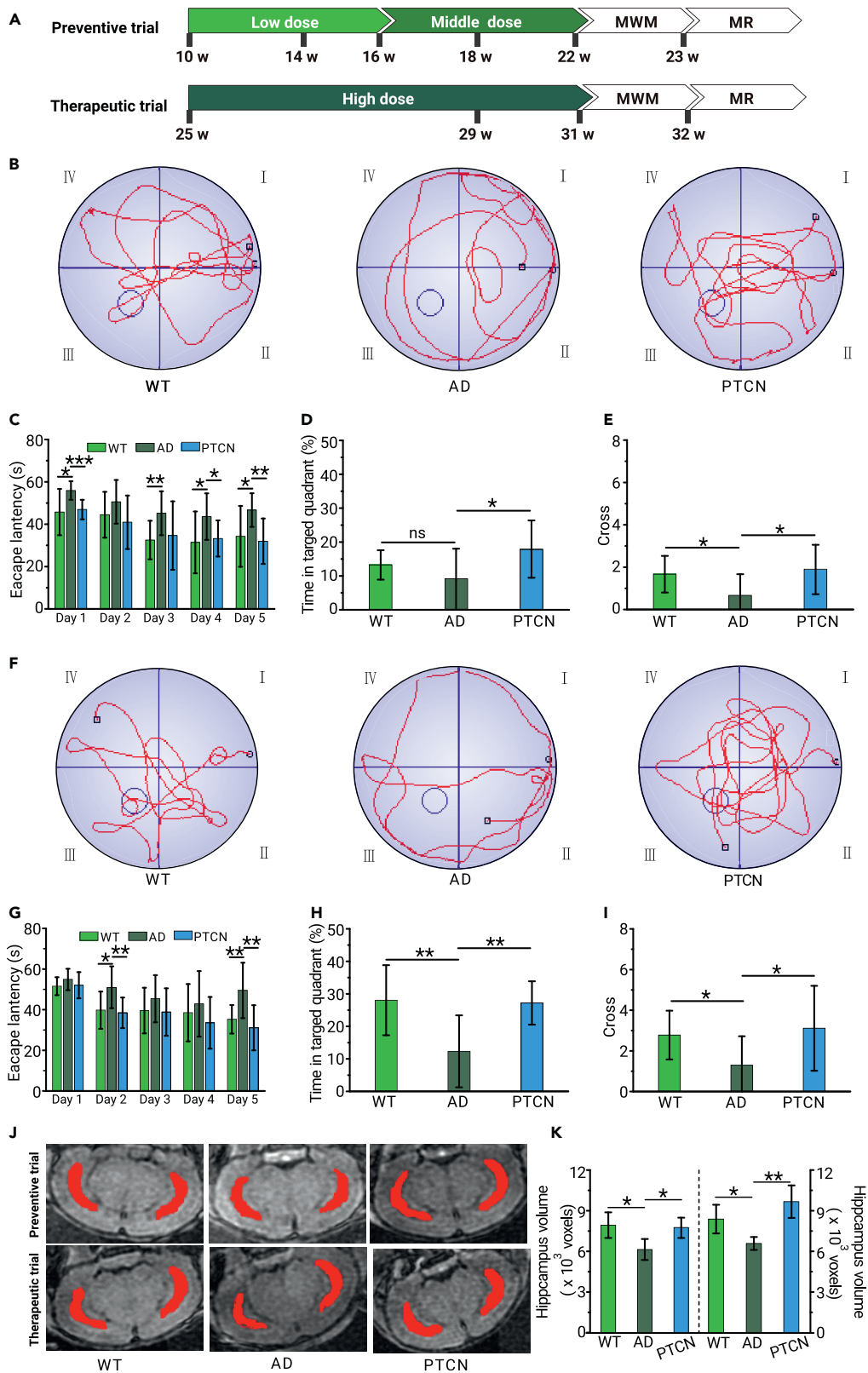


Figure 3. Behavioral and hippocampal volume evaluations for the preventive and therapeutic trials of PTCN *in vivo* (A) Time schedules for the preventive and therapeutic trials. (B) Representative swimming paths of mice in the preventive trial. (C–E) MWM results of the preventive trial: (C) Escape latency. (D) Swimming time spent in the targeted quadrant. (E) Number of times the mice cross over the platform site. In addition, we adjusted the legend of panels G–I as follows: (G–I) MWM results of the therapeutic trial; (G) Escape latency. (H) Swimming time spent in the targeted quadrant. (I) Number of times the mice cross over the platform site. (F) Representative swimming paths of mice in the therapeutic trial. (G–I) MWM results of the therapeutic trial. (J) T₁-weighted MRI of the mice brain and (K) corresponding analysis of hippocampal volume. WT, C57BL/6 mice; AD, APP/PS1 mice; PTCN, PTCN-treated APP/PS1 mice. For all graphs, the data are presented as the mean \pm SD and statistical significance was calculated by two-tailed t test; *p < 0.05, **p < 0.01, ***p < 0.001.

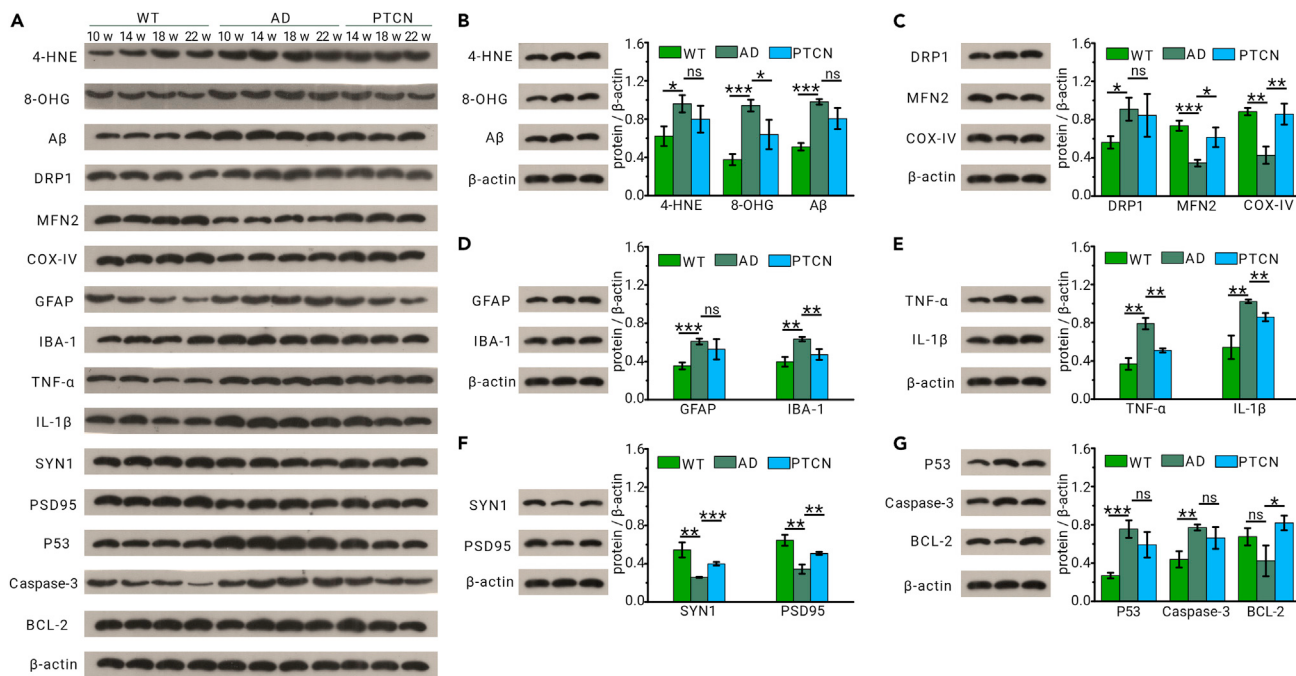


Figure 4. Pathological mechanism targeted by PTCN during the preventive trial *in vivo* (A) Representative immunoblots of AD-related pathological changes during the preventive trial from 10 to 22 weeks according to the time schedule. (B–G) Representative immunoblots and quantitative analysis of AD-related pathological changes in the preventive trial of PTCN at 23 weeks for (B) 4-HNE, 8-OHG, and A β ; (C) DRP1, mitofusin 2 (MFN2), and cytochrome c oxidase subunit IV (COX-IV); (D) GFAP and IBA-1; (E) TNF- α and IL-1 β ; (F) synapsin 1 (SYN1) and postsynaptic density protein 95 (PSD95); and (G) P53, caspase-3, and BCL-2. WT, C57BL/6 mice; AD, APP/PS1 mice; PTCN, PTCN-treated APP/PS1 mice. For all graphs, the data are presented as the mean \pm SD and statistical significance was calculated by two-tailed t test; *p < 0.05, **p < 0.01, ***p < 0.001.

for the therapeutic trial, APP/PPS1 mice at the age of 25 weeks were treated with a high dose until 31 weeks.

Cognitive behaviors were assessed with a Morris water maze (MWM) test (Figures 3B and 3F). To exclude the possible difference in sensorimotor functions between each group, the swimming speed of each group was first calculated and no significant difference was found among the three groups in both preventive and therapeutic trials (Figure S20). In both the preventive and therapeutic trials, the escape latency of PTCN-treated APP/PS1 mice was significantly shorter than that of untreated APP/PS1 mice (Figures 3C and 3G). Remarkably, both PTCN-treated APP/PS1 mice and wild-type (WT) mice showed a preference for the target quadrant, while untreated APP/PS1 mice rarely swam across it (Figures 3D and 3H). Similarly, PTCN treatment significantly increased the number of crossings of APP/PS1 mice over the platform in both the preventive and therapeutic trials (Figures 3E and 3I). Then, we evaluated hippocampal volume changes by magnetic resonance imaging (MRI) since hippocampal atrophy is a recognized biological marker of AD.^{33–35} In both the preventive and therapeutic trials, there were no differences in hippocampal volumes between PTCN-treated APP/PS1 mice and WT mice, while the volumes in untreated APP/PS1 mice were much smaller than those in WT mice (Figures 3J, 3K, and S21). Overall, these results suggest that, as AD progresses, cognitive impairment gradually worsens, and the impairment is accompanied by pronounced hippocampal atrophy; however, PTCN treatment through an adjustable gradient dosing strategy in the early and late stages of AD can effectively ameliorate cognitive impairments and hippocampal atrophy.

Ascertainment of the pathological mechanisms targeted by PTCN antioxidant treatment

To further explore the pathological mechanisms targeted by PTCN antioxidant treatment, pathological changes in the mouse hippocampus were detected monthly during both preventive (Figure 4A) and therapeutic trials (Figure 5A) by western blot analysis. First, lipid peroxidation and DNA oxidative damage represented by 4-hydroxynonenal (4-HNE) and 8-hydroxyguanine (8-OHG), respectively, were analyzed to evaluate the alleviation of OS by

PTCN. The 4-HNE assay results showed that 4-HNE appeared at 10 weeks in APP/PS1 mice and that the levels gradually increased (Figure 4A); however, the levels were slightly reduced after PTCN treatment in the preventive trial (Figure 4B). Notably, the levels of 4-HNE were higher in the older APP/PS1 mice than in the younger mice (Figure 5A) and were significantly reduced by PTCN treatment in the therapeutic trial (Figure 5B). The 8-OHG results showed that, during the preventive trial, a difference in 8-OHG level between APP/PS1 mice and WT mice appeared at 10 weeks, but the difference was gradually eliminated by PTCN treatment (Figures 4A and 4B). During the therapeutic trial, the 8-OHG level in APP/PS1 mice was quite high and was also greatly reduced by PTCN treatment to reach the same level as that in WT mice (Figures 5A and 5B). These results indicated that lipid peroxidation and DNA oxidative damage occurred at the beginning of the AD process and were gradually aggravated. PTCN treatment more effectively alleviated DNA oxidative damage than lipid peroxidation in the early stage of AD, while it alleviated both in the late stage of AD.

Next, we investigated other AD-related pathological changes that have been reported to interact with OS, including A β aggregates,³⁶ mitochondrial dysfunction,^{37,38} inflammation,³⁹ synaptic damage,⁴⁰ and neuronal apoptosis.⁴¹ PTCN treatment slightly but nonsignificantly reduced A β aggregates (Figures 4A, 4B, 5A, and 5B) in APP/PS1 mice. Given the apparent improvements in cognitive behavior and hippocampal volume, A β is very likely not the primary cause of cognitive impairments in AD, which is consistent with the fact that most clinical drugs for A β have failed. Obvious increases in dynamin-related protein 1 (DRP1) levels and decreases in mitofusin 2 and cytochrome c oxidase subunit IV levels were observed from 10 to 32 weeks in the hippocampus of APP/PS1 mice, indicating mitochondrial dysfunction (Figures 4A and 5A). PTCN treatment regulated the levels of mitochondrial function markers to close to normal levels, except for DRP1 (Figures 4C and 5C). The continuous activation of astrocytes and microglia as well as the increased levels of inflammatory cytokines in APP/PS1 mice indicated severe inflammation (Figures 4A and 5A). Notably, PTCN treatment markedly inhibited microglial activation and reduced inflammatory cytokine levels in the preventive trial but only slightly inhibited microglial activation and

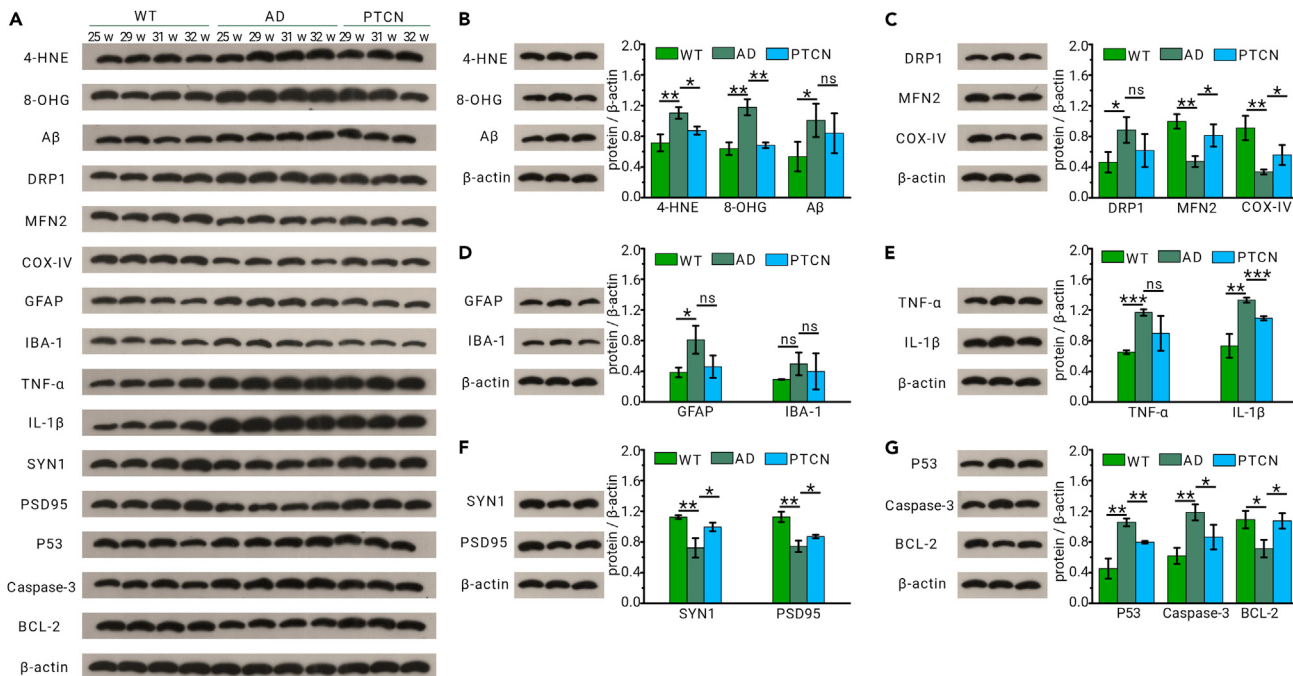


Figure 5. Pathological mechanism targeted by PTCN during the therapeutic trial *in vivo* (A) Representative immunoblots of AD-related pathological changes during the therapeutic trial from 25 to 32 weeks according to the time schedule. (B–G) Representative immunoblots and quantitative analysis of AD-related pathological changes in the therapeutic trial of PTCN at 32 weeks for (B) 4-HNE, 8-OHG, and A β ; (C) DRP1, MFN2, and COX-IV; (D) GFAP and IBA-1; (E) TNF- α and IL-1 β ; (F) SYN1 and PSD95; and (G) P53, caspase-3, and BCL-2. WT, C57BL/6 mice; AD, APP/PS1 mice; PTCN, PTCN-treated APP/PS1 mice. For all graphs, the data are presented as the mean \pm SD and statistical significance was calculated by two-tailed t test; *p < 0.05, **p < 0.01, ***p < 0.001.

reduced inflammatory cytokine levels in the therapeutic trial (Figures 4D, 4E, 5D and 5E). Marked synaptic damage represented by decreased levels of synapsin 1 and postsynaptic density protein 95 was observed in APP/PS1 mice (Figures 4A and 5A). As expected, continued deterioration was restrained by PTCN treatment in both the preventive and therapeutic trials (Figures 4F and 5F). Neuronal apoptosis was abnormal at 10 weeks in APP/PS1 mice, as characterized by increased levels of P53 and caspase-3 and decreased levels of BCL-2 (Figures 4A and 5A). In the preventive trial, P53 and caspase-3 levels were downregulated nonsignificantly, while BCL-2 levels were significantly upregulated after PTCN treatment (Figure 4G). In the therapeutic trial, the upregulation of BCL-2 as well as downregulation of P53 and caspase-3 was significantly observed after PTCN treatment (Figure 5G). So the mechanisms by which PTCN treatment attenuated neuronal death in the preventive trial and the therapeutic trial were considered to be different. Overall, PTCN counteracted mitochondrial dysfunction and synaptic damage during the entire process of AD. In the early stage of AD, PTCN also significantly inhibited inflammation and mildly inhibited neuronal apoptosis. In contrast, in the late stage of AD, PTCN weakly reduced inflammation but significantly enhanced apoptosis inhibition. These results demonstrate that PTCN administration via a gradient dosing strategy can effectively and continuously attenuate oxidative damage throughout different AD stages, thus attenuating other AD-related pathological mechanisms to varying degrees. These findings suggest that PTCN is a promising multitarget drug for both preventive and therapeutic treatments of AD.

Conclusion

In summary, PTCN, which consists of dual-targeted PTCN, was constructed for potential prevention and therapy of AD. Compared with the current nanotechnology to treat AD, the designed strategy in this study is superior in the following three aspects. Firstly, this work provides a simple and easy assembly of three traditional biomaterials. PB is a clinical therapeutic drug approved by the FDA, TF is a transporter of iron in human plasma that mediates BBB crossing, and CR is a common clinical diagnostic reagent for amyloidosis, all of which are widely used biomaterials and have good

biosafety for *in vivo* application. These three components are connected with chemical bonds to form multifunctional PTCN, revealing a new combination of traditional biomaterials. Our results validated the function of the above three components and demonstrated that PTCN with excellent biosafety could largely accumulate in AD lesions and exert substantial antioxidant effects. Secondly, this work first proposes an antioxidation-guided gradient dosing strategy that can be implemented throughout the course of AD from prevention to therapy. At present, the application of nanoantioxidant in AD treatment has gradually attracted attention, but most studies focus on the late treatment of severe cognitive impairment, and there is still a lack of research on early prevention and mild remission. In this work, the doses of PTCN can be adjusted according to the OS levels at different stages of the AD process, and the results showed that this strategy could effectively inhibit OS, ameliorate other pathological processes to varying degrees, and ultimately rescue cognitive impairment and hippocampal atrophy of APP/PS1 mice in both preventive and therapeutic trials. Finally, PTCN has great potential to be developed as a therapeutic drug and healthcare product for AD. As mentioned above, PTCN is an integration of three traditional biomaterials with a simple preparation method and high repeatability, and both *in vitro* and *in vivo* results have confirmed good biosafety of PTCN, which is conducive to future industrialization and clinical application. More importantly, PTCN can be applied to different stages of AD through the above antioxidation-guided gradient dosing strategy. We even hope that PTCN can be developed as a healthcare product similar to vitamins, which can be taken in a healthy state to prevent future occurrences. In addition to AD, the roles of OS in the occurrence and development of other diseases have received increasing attention,^{42–44} and PTCN may have considerable potential as a broad antioxidant for the treatment of various other OS diseases.

REFERENCES

- Ballard, C., Gauthier, S., Corbett, A., et al. (2011). Alzheimer's disease. *Lancet* **377**, 1019–1031.
- Jiang, T., Sun, Q., and Chen, S. (2016). Oxidative stress: a major pathogenesis and potential therapeutic target of antioxidative agents in Parkinson's disease and Alzheimer's disease. *Prog. Neurobiol.* **147**, 1–19.

3. Ahmad, W., Ijaz, B., Shabbiri, K., et al. (2017). Oxidative toxicity in diabetes and Alzheimer's disease: mechanisms behind ROS/RNS generation. *J. Biomed. Sci.* **24**, 76.
4. Cobley, J.N., Fiorello, M.L., and Bailey, D.M. (2018). 13 Reasons why the brain is susceptible to oxidative stress. *Redox Biol.* **15**, 490–503.
5. Valko, M., Leibfritz, D., Moncol, J., et al. (2007). Free radicals and antioxidants in normal physiological functions and human disease. *Int. J. Biochem. Cell Biol.* **39**, 44–84.
6. Wojsiat, J., Zoltowska, K.M., Laskowska-Kaszub, K., and Wojda, U. (2018). Oxidant/antioxidant imbalance in Alzheimer's disease: therapeutic and diagnostic prospects. *Oxidative Med. Cell. Longev.* **2018**, 6435861.
7. Sies, H., and Jones, D.P. (2020). Reactive oxygen species (ROS) as pleiotropic physiological signalling agents. *Nat. Rev. Mol. Cell. Biol.* **21**, 363–383.
8. Desai, P., Shete, H., Adnaik, R., et al. (2015). Therapeutic targets and delivery challenges for Alzheimer's disease. *World J. Pharmacol.* **4**, 236–264.
9. Zhang, Z.W., Xu, X.C., Liu, T., and Yuan, S. (2016). Mitochondrion-permeable antioxidants to treat ROS-burst-mediated acute diseases. *Oxid Med. Cell. Longev.* **2016**, 6859523.
10. Abbott, N.J., Patabendige, A.A., Dolman, D.E., et al. (2010). Structure and function of the blood-brain barrier. *Neurobiol. Dis.* **37**, 13–25.
11. Banks, W.A. (2019). The blood-brain barrier as an endocrine tissue. *Nat. Rev. Endocrinol.* **15**, 444–455.
12. Zhang, C., Wan, X., Zheng, X., et al. (2014). Dual-functional nanoparticles targeting amyloid plaques in the brains of Alzheimer's disease mice. *Biomaterials* **35**, 456–465.
13. Kwon, H.J., Cha, M.Y., Kim, D., et al. (2016). Mitochondria-targeting ceria nanoparticles as antioxidants for Alzheimer's disease. *ACS Nano* **10**, 2860–2870.
14. Singh, N., Savanur, M.A., Srivastava, S., et al. (2017). A redox modulatory Mn₃O₄ nanzyme with multi-enzyme activity provides efficient cytoprotection to human cells in a Parkinson's disease model. *Angew. Chem. Int. Ed. Engl.* **56**, 14267–14271.
15. Zhao, J., Cai, X., Gao, W., et al. (2018). Prussian blue nanzyme with multienzyme activity reduces colitis in mice. *ACS Appl. Mater. Inter.* **10**, 26108–26117.
16. Zhang, K., Tu, M., Gao, W., et al. (2019). Hollow Prussian blue nanzymes drive neuroprotection against ischemic stroke via attenuating oxidative stress, counteracting inflammation, and suppressing cell apoptosis. *Nano Lett.* **19**, 2812–2823.
17. Yang, Y., Brownell, C., Sadrieh, N., et al. (2007). Quantitative measurement of cyanide released from Prussian blue. *Clin. Toxicol.* **45**, 776–781.
18. Kim, L.D., and Factora, R.M. (2018). Alzheimer dementia: starting, stopping drug therapy. *Cleve. Clin. J. Med.* **85**, 209–214.
19. Williams, T.I., Lynn, B.C., Markey, W.R., and Lovell, M.A. (2006). Increased levels of 4-hydroxyneonenal and acrolein, neurotoxic markers of lipid peroxidation, in the brain in mild cognitive impairment and early Alzheimer's disease. *Neurobiol. Aging* **27**, 1094–1099.
20. Padurariu, M., Ciobica, A., Hritcu, L., et al. (2010). Changes of some oxidative stress markers in the serum of patients with mild cognitive impairment and Alzheimer's disease. *Neurosci. Lett.* **469**, 6–10.
21. Sultana, R., and Butterfield, D.A. (2010). Role of oxidative stress in the progression of Alzheimer's disease. *J. Alzheimers Dis.* **19**, 341–353.
22. Jack, C.R., Jr., and Holtzman, D.M. (2013). Biomarker modeling of Alzheimer's disease. *Neuron* **80**, 1347–1358.
23. Elahi, F.M., Casaleotto, K.B., La Joie, R., et al. (2020). Plasma biomarkers of astrocytic and neuronal dysfunction in early- and late-onset Alzheimer's disease. *Alzheimers Dement.* **16**, 681–695.
24. Sun, H., Liu, M., Sun, T., et al. (2019). Age-related changes in hippocampal ad pathology, actin remodeling proteins and spatial memory behavior of male APP/PS1 mice. *Behav. Brain Res.* **376**, 112182.
25. Zhang, W., Hu, S., Yin, J.J., et al. (2016). Prussian blue nanoparticles as multienzyme mimetics and reactive oxygen species scavengers. *J. Am. Chem. Soc.* **138**, 5860–5865.
26. Li, H., and Qian, Z.M. (2002). Transferrin/transferrin receptor-mediated drug delivery. *Med. Res. Rev.* **22**, 225–250.
27. Dapson, R.W. (2018). Amyloid from a histochemical perspective. A review of the structure, properties and types of amyloid, and a proposed staining mechanism for Congo red staining. *Biotech. Histochem.* **93**, 543–556.
28. Igħodaro, O.M., and Akinloye, O.A. (2019). First line defence antioxidants—superoxide dismutase (SOD), catalase (CAT) and glutathione peroxidase (GPX): their fundamental role in the entire antioxidant defence grid. *Alex. J. Med.* **54**, 287–293.
29. Shi, C., Li, Y., and Gu, N. (2020). Iron-based nanzymes in disease diagnosis and treatment. *ChemBioChem* **21**, 2722–2732.
30. Yao, J., Cheng, Y., Zhou, M., et al. (2018). ROS scavenging Mn₃O₄ nanzymes for *in vivo* anti-inflammation. *Chem. Sci.* **9**, 2927–2933.
31. Qin, Z., Li, Y., and Gu, N. (2018). Progress in applications of Prussian blue nanoparticles in biomedicine. *Adv. Healthc. Mater.* **7**, e1800347.
32. Qi, S., Feng, Z., Li, Q., et al. (2018). Inhibition of ROS-mediated activation Src-MAPK/AKT signaling by orientin alleviates H₂O₂-induced apoptosis in PC12 cells. *Drug Des. Devel. Ther.* **12**, 3973–3984.
33. Pini, L., Pievani, M., Bocchetta, M., et al. (2016). Brain atrophy in Alzheimer's disease and aging. *Ageing Res. Rev.* **30**, 25–48.
34. Matsuda, H. (2016). MRI morphometry in Alzheimer's disease. *Ageing Res. Rev.* **30**, 17–24.
35. Nadal, L., Coupe, P., Helmer, C., et al. (2020). Differential annualized rates of hippocampal subfields atrophy in aging and future Alzheimer's clinical syndrome. *Neurobiol. Aging* **90**, 75–83.
36. Cheignon, C., Tomas, M., Bonnefont-Rousselot, D., et al. (2018). Oxidative stress and the amyloid beta peptide in Alzheimer's disease. *Redox Biol.* **14**, 450–464.
37. Yan, M.H., Wang, X., and Zhu, X. (2013). Mitochondrial defects and oxidative stress in Alzheimer disease and Parkinson disease. *Free Radic. Biol. Med.* **62**, 90–101.
38. Burte, F., Carelli, V., Chinnery, P.F., and Yu-Wai-Man, P. (2015). Disturbed mitochondrial dynamics and neurodegenerative disorders. *Nat. Rev. Neurol.* **11**, 11–24.
39. Bostancıklıoglu, M. (2019). An update on the interactions between Alzheimer's disease, autophagy and inflammation. *Gene* **705**, 157–166.
40. Scheff, S.W., Ansari, M.A., and Mufson, E.J. (2016). Oxidative stress and hippocampal synaptic protein levels in elderly cognitively intact individuals with Alzheimer's disease pathology. *Neurobiol. Aging* **42**, 1–12.
41. Circu, M.L., and Aw, T.Y. (2010). Reactive oxygen species, cellular redox systems, and apoptosis. *Free Radic. Biol. Med.* **48**, 749–762.
42. Barnes, P.J., Burney, P.G., Silverman, E.K., et al. (2015). Chronic obstructive pulmonary disease. *Nat. Rev. Dis. Primers* **1**, 15076.
43. Tan, Y., Zhang, Z., Zheng, C., et al. (2020). Mechanisms of diabetic cardiomyopathy and potential therapeutic strategies: preclinical and clinical evidence. *Nat. Rev. Cardiol.* **17**, 585–607.
44. Zhang, Y., Murugesan, P., Huang, K., and Cai, H. (2020). NADPH oxidases and oxidase crosstalk in cardiovascular diseases: novel therapeutic targets. *Nat. Rev. Cardiol.* **17**, 170–194.

ACKNOWLEDGMENTS

This work was supported by the National Natural Science Foundation of China (51873150, 51573128).

AUTHOR CONTRIBUTIONS

Y.D., J.C., and D.Z. conceived and designed the experiments. D.Z. conducted most experiments. Y.T. helped with experiments in cells and MWM test. X.S. performed the detection of hippocampal volume and contributed analysis tools in MRI. C.Z. helped with flow cytometer analysis. Y.D. and D.Z. analyzed the data and wrote the paper.

DECLARATION OF INTERESTS

The authors declare no competing interests.

SUPPLEMENTAL INFORMATION

Supplemental information can be found online at <https://doi.org/10.1016/j.xinn.2021.100160>.

LEAD CONTACT WEBSITE

http://faculty.tju.edu.cn/966357/zh_CN/index.htm